Munk W, Worcester P and Wunsch C (1995) *Ocean Acoustic Tomography*. Cambridge: Cambridge University Press.
Parker RL (1994) *Geophysical Inverse Theory*. Princeton, NJ: Princeton University Press.
Seber GAF (1977) *Linear Regression Analysis*. New York: Wiley.
Tarantola A (1987) *Inverse Problem Theory. Methods for Data Fitting and Model Parameter Estimation*. Amsterdam: Elsevier.
Van Trees HL (1968) *Detection, Estimation and Modulation Theory. Part I*. New York: Wiley.
Wiggins RA (1972) The general linear inverse problem: implication of surface waves and free oscillations for earth structure. *Reviews in Geophysics and Space Physics* 10: 251–285.
Wunsch C (1977) Determining the general circulation of the oceans: a preliminary discussion. *Science* 196: 871–875.
Wunsch C (1994) Dynamically consistent hydrography and absolute velocity in the eastern North Atlantic Ocean. *Journal of Geophysical Research* 99: 14071–14090.
Wunsch C (1996) *The Ocean Circulation Inverse Problem*. Cambridge: Cambridge University Press.

IR RADIOMETERS

C. J. Donlon, Space Applications Institute, Ispra, Italy

doi:10.1006/rwos.2001.0332

Introduction

Measurements of sea surface temperature (SST) are most important for the investigation of the processes underlying heat and gas exchange across the air–sea interface, the surface energy balance, and the general circulation of both the atmosphere and the oceans. Complementing traditional subsurface contact temperature measurements, there is a wide variety of infrared radiometers, spectroradiometers, and thermal imaging systems that can be used to determine the SST by measuring thermal emissions from the sea surface. However, the SST determined from thermal emission can be significantly different from the subsurface temperature ($> \pm 1$ K) because the heat flux passing through the air–sea interface typically results in a strong temperature gradient. Radiometer systems deployed on satellite platforms provide daily global maps of SSST (sea surface temperature) at high spatial resolution (~ 1 km) whereas those deployed from ships and aircraft provide data at small spatial scales of centimeters to meters. In particular, the development of satellite radiometer systems providing a truly synoptic view of surface ocean thermal features has been pivotal in the description and understanding of the global oceans.

This article reviews the infrared properties of water and some of the instruments developed to measure thermal emission from the sea surface. It focuses on *in situ* radiometers although the general principles described are applicable to satellite sensors treated elsewhere in this volume.

Infrared Measurement Theory

Infrared (IR) radiation is heat energy that is emitted from all objects that have a temperature above 0 K (-273.16°C). It includes all wavelengths of the electromagnetic spectrum between 0.75 μm and ~ 100 μm (**Figure 1**) and has the same optical properties as visible light, being capable of reflection, refraction, and forming interference patterns.

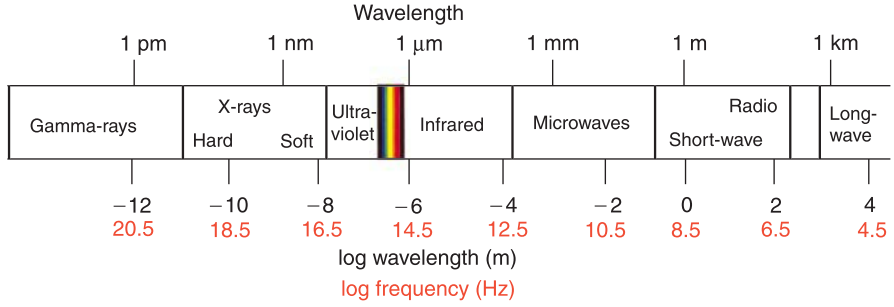

Figure 1 Schematic diagram of the electromagnetic spectrum showing the location and interval of the infrared waveband.

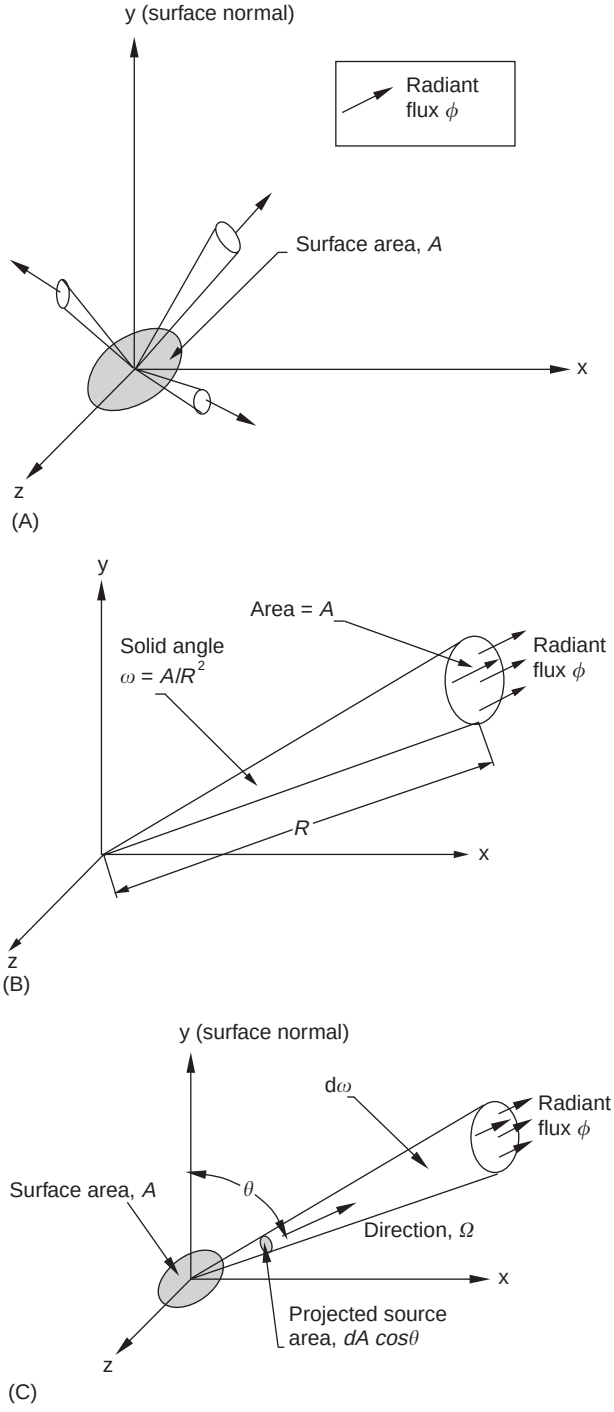

Figure 2 Schematic definition of (A) Emittance, *E*; (B) radiant intensity, *I*; (C) radiance, *L*.

The following total quantities, conventional symbols and units provide the theoretical foundation for the measurement of IR radiation and are schematically shown in **Figure 2**. Spectral quantities can be represented by restricting each to a specific waveband.

- Radiant energy Q, is the total energy radiated from a point source in all directions in units of joules (J).
- Radiant flux $\phi = dQ/dt$ is the flux of all energy radiated in all directions from a point source in units of watts (W).
- Emittance $M = d\phi/dA$ is the radiant flux density from a surface area A in units of $W\,m^{-2}$. This is an integrated flux (i.e., independent of direction) and will therefore vary with orientation relative to a nonuniform source.
- Radiant intensity $I = d\phi/d\omega$ is the radiant flux of a point source per solid angle ω (steradian, sr) and is a directional flux in units of $W\,sr^{-1}$.
- Radiance $L = dI/d(A\cos\theta)$ is the radiant intensity of an extended source per unit solid angle in a given direction θ, per unit area of the source projected in the same θ. It has units of $W\ sr^{-1}\,m^{-2}$.

Planck's law describes the emittance of a perfectly emitting surface (or black body) at a temperature T in Kelvin. It is the radiant flux (ϕ) per unit bandwidth centered at wavelength λ leaving a unit area of surface in any direction in units of $W\,m^{-2}\,m^{-1}$.

$$M_{(\lambda,T)} = \frac{2\pi hc^2}{\lambda^5(e^{hc/\lambda kT} - 1)} \qquad [1]$$

where $h = 6.626 \times 10^{-34}\,J\,s$ is Planck's constant, $c = 2.998 \times 10^{8}\,m\,s^{-1}$ is the speed of light and $k = 1.381 \times 10^{-23}\,J\,K^{-1}$ is Boltzmann's constant. The sea surface is considered a Lambertian source (i.e., uniform radiance in all directions) so that the spectral radiance L_λ is related to M_λ by

$$L_\lambda = \frac{M_\lambda}{\pi} \qquad [2]$$

Figure 3 shows L_λ computed for several temperatures as a function of wavelength. Considering temperatures of 273–310 K as representative of the global ocean, maximum emission occurs at a wavelength of 9.3–10.7 μm. Atmospheric attenuation is minimal at $\sim$3.5 μm, 9.0 μm and 11.0 μm that are the spectral intervals often termed atmospheric 'windows'. Instruments operating within these intervals are optimal for sea surface measurements – especially in the case of satellite deployment where atmospheric attenuation can be significant. In the 3–5 μm spectral region. L_λ is a strong function of temperature (**Figure 3**) highlighting the possibility to increase in radiometer sensitivity by utilizing this spectral interval.

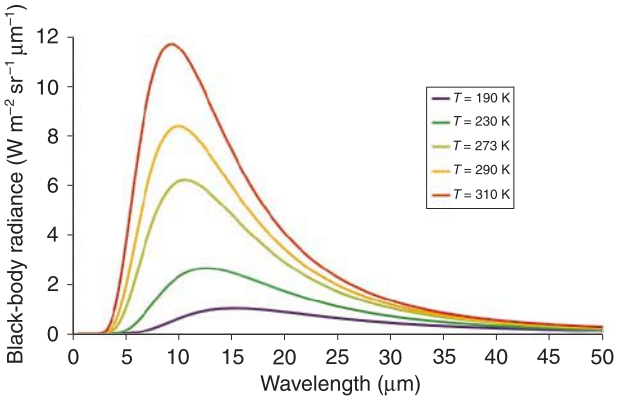

Figure 3 Black-body radiance as a function of wavelength computed using eqns [1] and [2] for different target temperatures.

By measuring L_λ using eqn [2] and inverting eqn [1], the spectral brightness temperature, $B_{(T,\lambda)}$, rather than the temperature is determined because these equations assume that sea water is a perfect emitter or black body. In practice, the sea surface does not behave as a black body (it is slightly reflective in the infrared) and therefore its spectral and geometric properties need to be considered. The emittance of a perfect emitter at the actual temperature T, wavelength λ, and view angle θ is given by

$$M_{(T,\lambda,\theta)} = \frac{\pi L_{(T,\lambda,\theta)}}{\varepsilon_{(\lambda,\theta)}} \quad [3]$$

where the emissivity, $\varepsilon_{(\lambda,\theta)}$, can be calculated using

$$\varepsilon_{(\lambda,\theta)} = \frac{M_{(T,\lambda,\theta)}measured}{M_{(T,\lambda,\theta)}blackbody} \quad [4]$$

which has a strong dependence on wavelength and viewing geometry. The effective emissivity, ε, integrates $\varepsilon_{(\lambda,\theta)}$ over all wavelengths of interest for radiometer view angle θ. **Figure 4A** shows the calculated normal reflectivity, ρ, of pure water as a function of wavelength for the spectral region 1–100 μm. Pure water differs only slightly from sea water in this context. Note that ρ is minimal at a wavelength of $\sim 11\,\mu m$ ($\rho \approx 0.0015$) and following Kirchoff's law

$$\rho_\lambda + \tau_\lambda + \varepsilon_\lambda = 1 \quad [5]$$

where ρ_λ is the spectral reflectivity and τ_λ is the spectral transmissivity. The e-folding penetration depth (i.e., the depth of 63% emission) or optical depth at a typical wavelength of 11 μm is $\approx 10\,\mu m$, τ_λ can be neglected and ε_λ can be calculated using

$$\varepsilon_\lambda = 1 - \rho_\lambda \quad [6]$$

Although the actual optical depth is wavelength dependent, it is clear that IR radiometers determine the temperature of a very thin 'skin' layer of the ocean. This temperature is termed the sea surface skin temperature (SSST) and is distinct (although related) to the subsurface SST. Note that this is in contrast to the situation for short-wave solar radiation (having wavelengths of ~ 0.4–$0.7\,\mu m$) which, for clear water, penetrates to a depth of $\sim 100\,m$.

Figure 4B shows the ε_λ of pure water computed from eqn [6] as a function of both viewing zenith angle and spectral wavelength. Inspection of **Figure 4** reveals that the best radiant temperature measurement will be made when viewing a calm sea surface at an angle of 0–40° from nadir.

An IR radiometer is an optical instrument designed to measure L_λ entering an instrument aperture (**Figure 5**). The radiance measured by radiometer, $L_{(T,\lambda,\theta)}$, having a spectral bandwidth λ, viewing the sea surface at a zenith angle θ and temperature T is given by:

$$L_{(T,\lambda,\theta} = \int_0^\alpha \xi_\lambda [\varepsilon_{(\lambda,\theta)} B(T_{surf},\lambda) + (1 - \varepsilon_{(\lambda,\theta)}) B(T_{atm},\lambda) + L_{path(b,\lambda,\theta)}] d\lambda \quad [7]$$

where ξ_λ is the spectral response of the radiometer, $B(T_{surf},\lambda)$ and $B(T_{atm},\lambda)$are the Planck function for surface temperature T_{surf}, and atmospheric temperature T_{atm}, and $L_{path(b,\lambda,\theta)}$ is the radiance emitted by the atmosphere between the radiometer at height h above the sea surface reflected into the radiometer field-of-view (FoV) at the sea surface. Note that the horizontal and vertical polarization components of reflectivity shown in **Figure 4** are unequal. It is important to consider the polarization of surface reflectance when making measurements of the sea surface because diffuse downwelling sky radiance measured by a radiometer after reflection at the sea surface is polarized.

IR Radiometer Design

There are four fundamental components to all IR radiometer instruments described below.

Detector and Electronics System to Measure Radiance and Control the Radiometer

A detector system provides an output proportional to the target radiance incident on the detector.

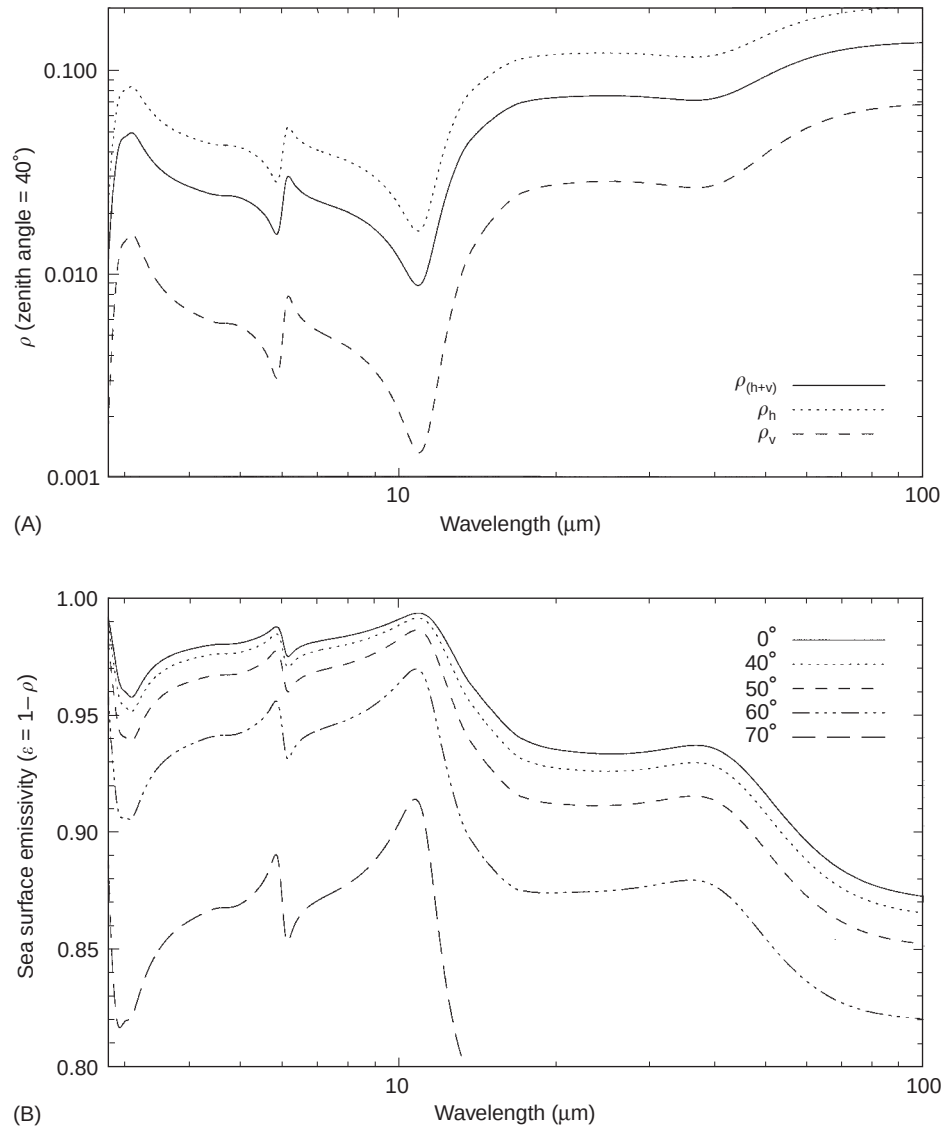

Figure 4 (A) The normal reflectivity, ρ, of the pure water as a function of wavelength (full line). Also shown are the horizontal polarized (ρ_h) and the vertically polarized (ρ_v) components of ρ. (B) The spectral emissivity of pure water as a function of viewing zenith angle. *h*, height above sea surface.

There are two main types of detector: thermal detectors that respond to direct heating and quantum detectors that respond to a photon flux. In general, thermal detectors have a response that is weakly dependent on wavelength and can be operated at ambient temperatures whereas rapid response quantum detectors require cooling and are wavelength dependent.

Fore-optics System to Filter, Direct and Focus Radiance

All optical components have an impact on radiometer reliability and accuracy. Mirrors should be free of aberration to minimize unwanted stray radiance reaching the detector. Several materials have good reflection characteristics in the IR including, gold, polished aluminum, and cadmium. Care should be exercised when choosing an appropriate mirror substrate and reflection coating to avoid decay in the marine atmosphere. A glass substrate having a 'hard' scratch-resistant polished gold surface provides $> 98\%$ reflectance and good environmental wear.

Spectral filter windows and lenses require spectral properties that, together with the detector characteristics, define the overall spectral characteristics of a radiometer. **Figure 6** shows the combined spectral

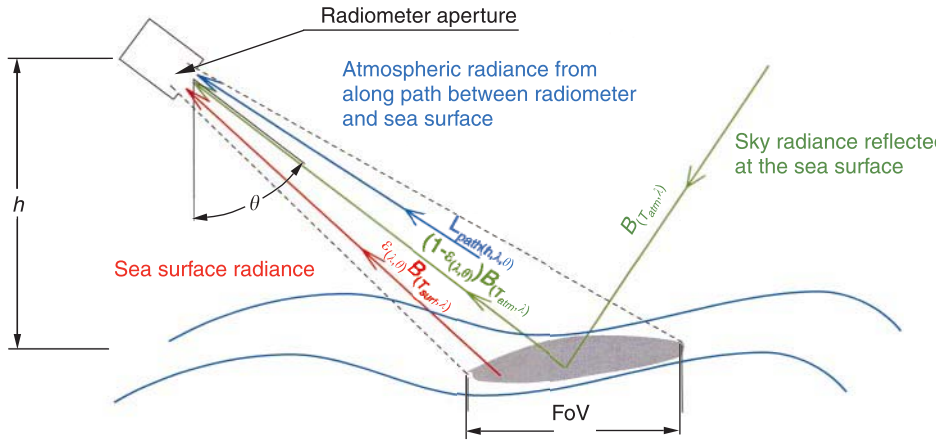

Figure 5 Schematic diagram showing the radiance components measured by an IR radiometer viewing the sea surface. Fov, Field of view.

response for a broadband radiometer together with the component spectral response of the window and detector.

Environmental System to Protect and Thermally Stabilize the Radiometer

For any optical instrument intended for use in the harsh marine environment, adequate environmental protection is critical. Rain, sea-water spray, and high humidity can destroy a poorly protected instrument rapidly and components such as electrical connections and fore-optics should be resistant to these effects. *In situ* radiometer windows are particularly important in this context. They should not significantly reduce the incoming signal or render it noisy, and be strong enough to resist mechanical, thermal and chemical degradation. **Figure 7** describes several common materials. Germanium (Ge) windows have good transmission characteristics but are very brittle. Sodium chloride (NaCl) is a low-cost, low-absorption material but is of little use in the marine environment because it is water-soluble.

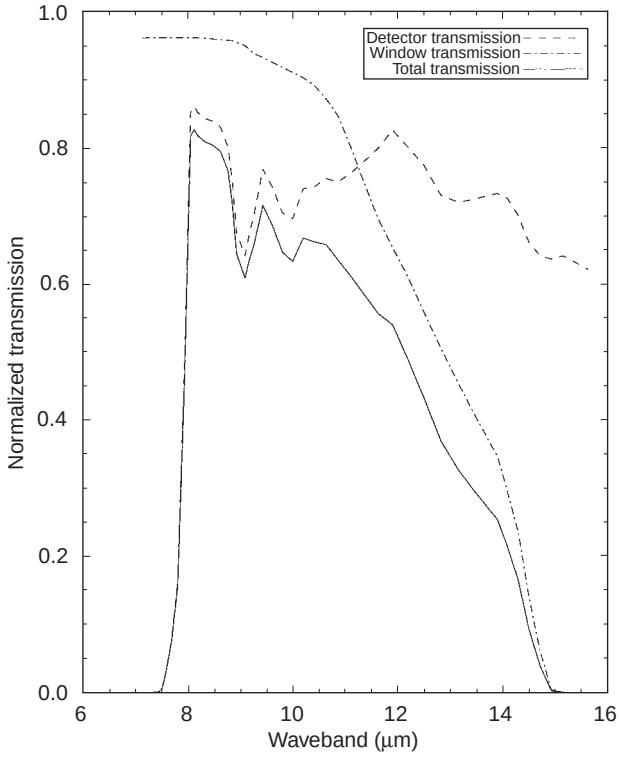

Figure 6 Normalized spectral transmission of an IR window and detector shown together with the combined total response.

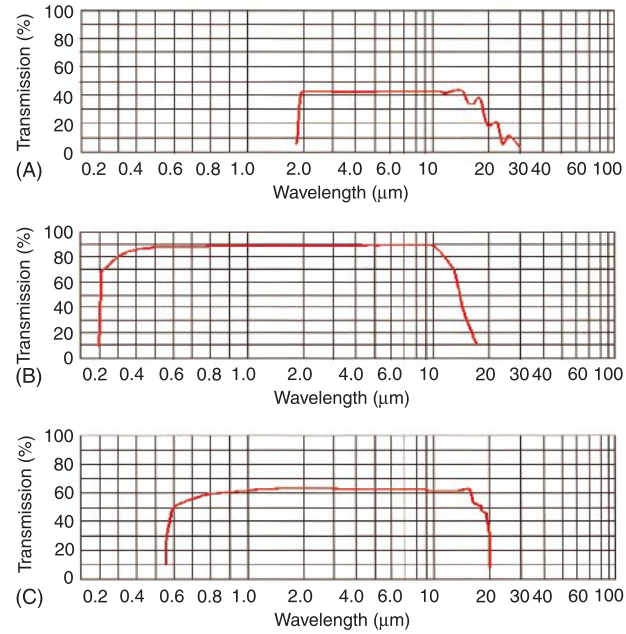

Figure 7 Spectral transmission for common IR window materials. (A) Germanium, (B) sodium chloride, (C) zinc selenide.

Zinc selenide (ZnSe) has high transmission, is non-hygroscopic and resistant to thermal shock but is soft and requires a protective 'hard' surface finish coating.

Certain window materials achieve better performance when antireflection (AR) coatings are used to minimize reflection from the window. For example, when an AR coating is used on a ZnSe window the transmission increases from $\sim 70\%$ to $\sim 90\%$. Other coatings provide windows that polarize the incident radiance signal such as optically thin interference coatings and wire grid diffraction polarizers.

Deposition of marine NaCl on all optical components (especially calibration targets) presents an unavoidable problem. Although NaCl itself has good infrared transmission properties (**Figure 7**), contaminated surfaces may become decoupled from temperature sensors and the noise introduced by the optical system will increase. Finally, adequate thermal control using reflective paint together with substantial instrument mass is required so that instruments are not sensitive to thermal shock. In higher latitudes, it may be necessary to provide an extensive antifreeze capability.

Calibration System to Quantify the Radiometer Output

The role of a calibration system is to quantify the instrument output in terms of the measured radiance incident on the detector. Calibration techniques are specific to the particular design of radiometer and vary considerably from simple bias corrections to systems providing automatic precision two-point blackbody calibrations. Proper calibration accounts for the following primary sources of error:

- the effect of fore-optics;
- unavoidable drifts in detector gain and bias;
- long-term degradation of components.

Finally, careful radiometer design and configuration can avoid many measurement errors. Examples include: poor focusing and optical alignment; filters having transmission above or below the stated spectral bandwidth (termed 'leaks'); inadequate protection against thermal shock, stability, and reliability of the calibration system; poor electronics and the general decay of optomechanical components.

Application of IR Radiometers

There are many different radiometer designs and deployment strategies ranging from simple single-channel hand-held devices to complex spectro-radiometers. Instrument accuracy, sensitivity and stability depends on both the deployment scenario and radiometer design. Accordingly, the following sections describe several different examples.

Broadband Pyrgeometers

A pyrgeometer is an integrating hemispheric radiometer which, by definition, measures the band-limited spectral emittance, E, so that the angle dependency in eqn [7] is redundant. They are used to determine the long-wave heat flux at the air–sea interface by measuring the difference between atmospheric and sea surface radiance either using two individual sensors (**Figure 8A**) or as a single combined sensor (**Figure 8B**). A thermopile detector is often used which is a collection of thermocouple detectors composed of two dissimilar metallic conductors connected together at two 'junctions.' The measurement junction is warmed by incident radiance relative to a stable reference junction and a μV signal is produced. The response of a thermopile has little wavelength dependence and a hemispheric dome having a filter (~ 3–$50\,\mu m$) deposited on its inner surface typically defines the spectral response. Direct compensation for thermal drift using a temperature sensor located at the thermopile reference junction is sometimes used but regular calibration using an independent laboratory blackbody is mandatory. An accuracy of $< 10\,W\,m^{-2}$ is possible

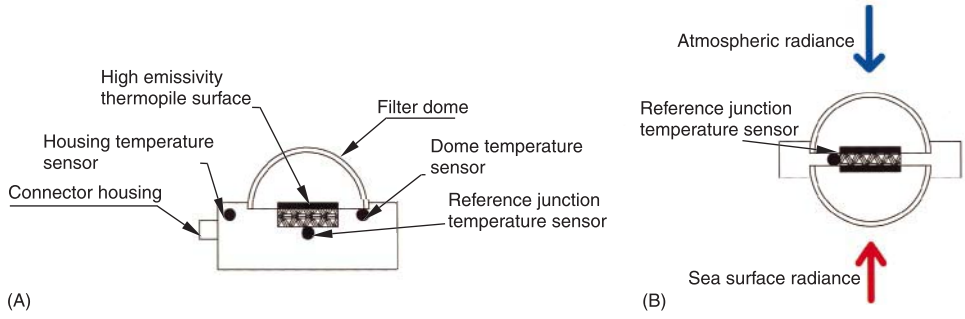

Figure 8 (A) A typical design of a long-wave pyrgeometer. (B) A net-radiation pyrgeometer for determination of the net long-wave flux at the sea surface.

after significant correction for instrument temperature drift and stray radiance contribution using additional on-board temperature sensors.

Narrow Beam Filter Radiometers

Narrow beam filter radiometers are often used to determine the SSST for air–sea interaction studies and for the validation of satellite derived SSST and there are several low-cost instruments that provide suitable accuracy and spectral characteristics. Many of these use a simple thermopile or thermistor detector together with a low-cost broadband-focusing lens. Typically, they have simple self-calibration techniques based on the temperature of the instrument and/or detector. Consequently they have poor resistance to thermal shock and have fore-optics that readily degrade in the marine atmosphere. However, handled with care, these devices are accurate to $\pm 0.1\,\mathrm{K}$, albeit with limited sensitivity.

Precision narrow beam filter radiometers often use pyroelectric detectors that produce a small electrical current in response to changes in detector temperature forced by incident radiation. They have a fast response at ambient temperatures but require a modulated signal to operate. Modulation is accomplished by using an optical chopper having high reflectivity 'vanes' to alternately view a reference radiance source by reflection and a free path to the target radiance. The most common chopper systems are rotary systems driven by a small electric motor phase locked to the detector output by an optoelectronic sensor **Figure 9A**. An alternative design driven by a small oscillating electromagnetic coil called a tuning fork chopper is shown in **Figure 9B**. As the coil resonates, the reflective vanes of the chopper oscillate alternately opening and closing an aperture 'gap.'

Dynamic detector bias compensation is inherent when using an optical chopper. The detector alternately measures radiance from the sea surface L_{src} and a reference blackbody, L_{bb} (sometimes this is the detector itself) reflected by the chopper vanes resulting in two signals

$$S_1 = L_{bb} + \delta \qquad [8]$$

$$S_2 = L_{src} + \delta \qquad [9]$$

Assuming L_{bb} remains constant during a short chopping cycle, the bias term δ in eqns [8] and [9] is eliminated

$$\Delta S = S_1 - S_2 = L_{bb} - L_{src} \qquad [10]$$

It is important to recognize the advantages to this technique, which is widely used:

- There is minimal thermal drift of the detector;
- The detector is dynamically compensated for thermal shock;
- A precise modulated signal is generated well suited to selective filtering providing excellent noise suppression and signal stability.

However, in order to compensate for instrument gain changes, an additional blackbody sources(s) is required. These are periodically viewed by the detector to provide a mechanism for absolute calibration. Either the black body is moved into the detector FoV or an adjustable mirror reflects radiance from the black body on to the detector. Calibration cycles should be made at regular intervals so that gain changes can be accurately monitored and calibration sources need to be viewed using the same optical path as that used to view the sea surface.

A basic 'black-body' calibration strategy uses an external bath of sea water as a high ε (>0.95)

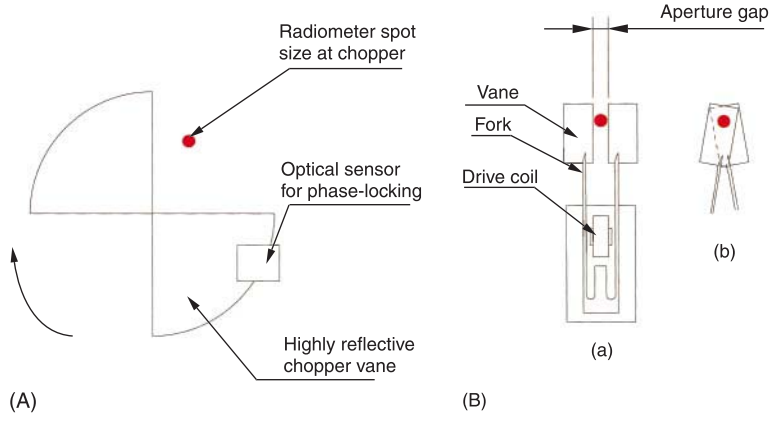

Figure 9 (A) Schematic layout of a rotary chopper; (B) schematic layout of a tuning fork chopper, (a) open, (b) closed.

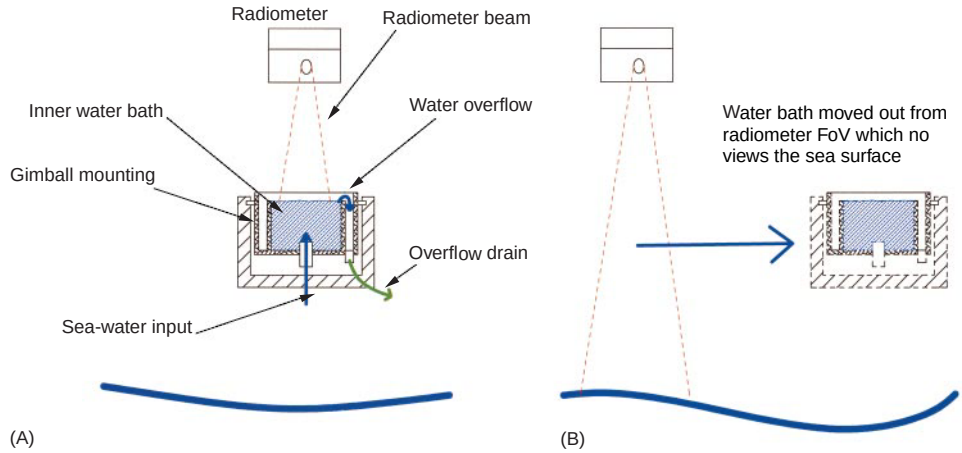

Figure 10 Schematic diagram showing the stirred water bath calibration scheme. (A) The radiometer in calibration mode, (B) the radiometer viewing the sea surface after the water bath has been moved out of the field of view (FoV).

reference as shown in **Figure 10**. In this scheme, the radiometer periodically views the water bath that is stirred vigorously to prevent the development of a thermal skin temperature deviation. The view geometry for the water bath and the sea surface are assumed to be identical and, by measuring the temperature of the water bath the radiometer can be absolutely calibrated. An advantage of this technique is that $\varepsilon_{(\lambda,\theta)}$ is not required to determine the SSST. However, in practice, it is difficult to continuously operate a water bath at sea and surface roughness differences between the bath and sea surface are ignored.

On reflection at the sea surface, diffuse sky radiance is polarized and, at Brewster's angle ($\sim 50^\circ$ from nadir at a wavelength of 11 μm), the vertical v-polarization is negligible for a given wavelength (**Figure 11**). Only the horizontal h-polarization component remains so that if the radiometer filter response is v-polarized (i.e., only passes v-polarized radiance), negligible reflected sky radiance is measured by the radiometer. In practice, because Brewster's angle is very sensitive to the geometry of a particular deployment (approximately $\pm 2^\circ$) this technique is only applicable to deployments from fixed platforms and when the sea surface is relatively calm. Further, the use of a polarizing filter will significantly reduce the signal falling on the detector increasing the signal-to-noise ratio.

The use of fabricated black-body cavities (**Figure 12A**) provides an accurate, versatile and, compact calibration system. Normally, two black-body cavities are used, one of which follows the ambient temperature of the instrument and a second is heated to a nominal temperature above this. High ε (> 0.99) is attained by a combination of specialized surface finish and black-body geometry. The cavity radiance is determined as a function of the black body temperature that is easily measured. **Figure 12B** shows a schematic outline of a typical black-body radiometer design using a rotary chopper and **Figure 12C** provides a schematic diagram of a typical output signal.

Note that for all calibration schemes, larger errors are expected beyond the calibrated temperature range which can be a problem for sky radiance

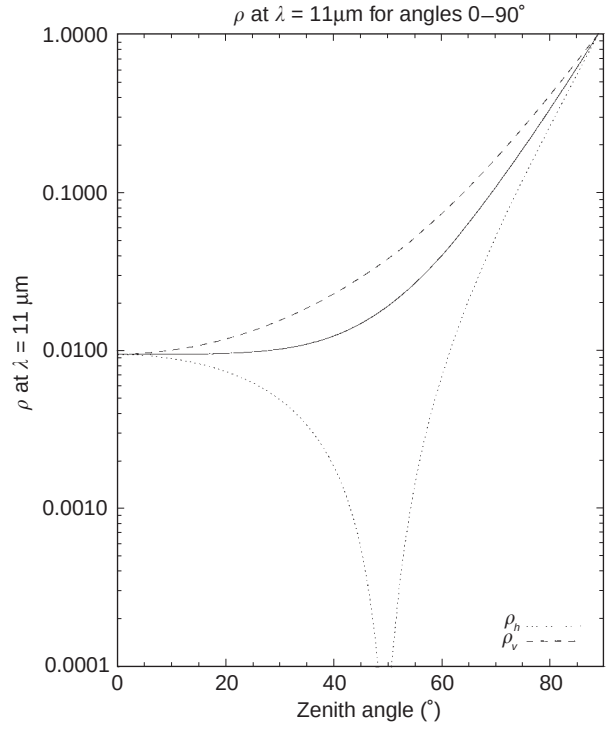

Figure 11 Polarization of sea surface reflection at 11 μm as a function of view angle. Total polarization is shown as a solid line.

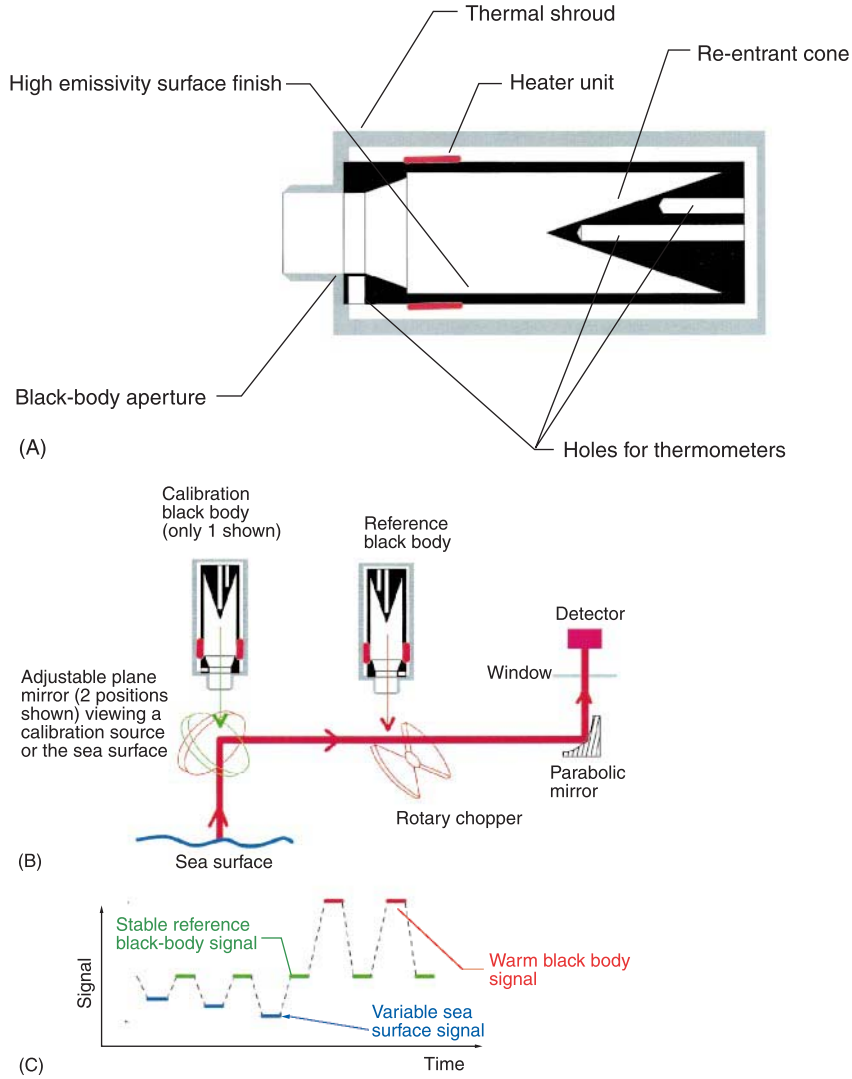

Figure 12 (A) A section through a black-body calibration cavity of the re-entrant cone design. (B) A typical black-body calibration radiometer using a rotary optical chopper. (C) A schematic diagram of a typical detector output signal, showing sea, reference, and calibration signals.

measurements where clear sky temperatures of $< 200\,\mathrm{K}$ are common.

Multichannel Radiometers

The terms in eqn [7] are directly influenced by the height, h, of the radiometer above the sea surface and are different in magnitude for *in situ* and spacecraft deployments. In the case of a sea surface *in situ* radiometer deployment, $L_{path(h,\lambda,\theta)}$ is typically neglected because h is normally $< 10\,\mathrm{m}$ unless the atmosphere has a heavy water vapor loading (e.g., $> 90\%$) or an aircraft deployment is considered. However, for a spacecraft deployment, this is a significant term requiring explicit correction. Conversely, the $B(T_{atm},\lambda)$ term is critical to the accuracy of an *in situ* radiometer deployment but of little impact (except perhaps at the edge of clouds) for a satellite instrument deployment because $L_{path(h,\lambda,\theta)}$ dominates the signal. A multispectral capability can be used to explicitly account for $L_{path(h,\lambda,\theta)}$ in eqn [7] because of unequal atmospheric attenuation for different spectral wavebands. Multichannel radiometers are exclusively used on satellite platforms for this reason. Many *in situ* multichannel radiometers are designed primarily for the radiant calibration or validation of specific satellite radiometers and the development of satellite radiometer atmospheric correction algorithms. They often have several selectable filters matched to those of the satellite sensor,

It is worth noting that multiangle view radiometers are also capable of providing an explicit correction for atmospheric attenuation. Often

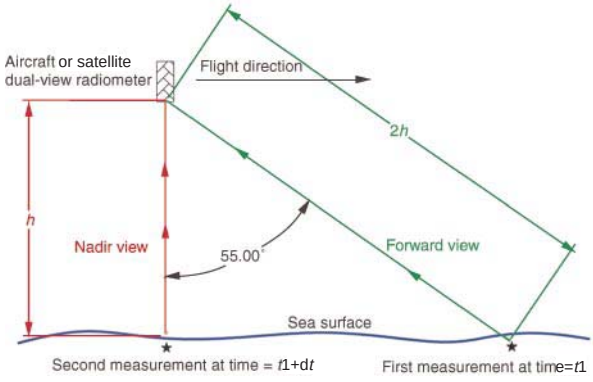

Figure 13 Schematic diagram of dual view, double atmospheric path radiometer deployment geometry.

operated from satellite and aircraft, these instruments provide a direct measure of atmospheric attenuation by making two views of the same sea surface area at different angles using a geometry that doubles the atmospheric pathlength (**Figure 13**). The assumption is made that atmospheric and oceanic conditions are stationary in the time between each measurement.

Spectroradiometers

A recent development is the use of Fourier transform infrared spectrometers (FTIR) that are capable of accurate ($\sim 0.05\,\mathrm{K}$). high spectral resolution ($\sim 0.5\,\mathrm{cm}^{-1}$) measurements over a broad spectral range (typically ~ 3–$18\,\mu\mathrm{m}$) as shown in **Figure 14**. The FTIR provides a unique tool for the development of new IR measurement techniques and investigation of processes at the air–sea interface. For example, the Marine-Atmospheric Emitted Radiance Interferometer (M-AERI) has pioneered a SSST algorithm that uses a narrow spectral region centered at $7.7\,\mu\mathrm{m}$ that is less susceptible to the influence of cloud cover and sky emissions that at 10–$12\,\mu\mathrm{m}$. The FTIR can also be used to measure air temperatures by viewing the atmosphere at $\sim 15\,\mu\mathrm{m}$

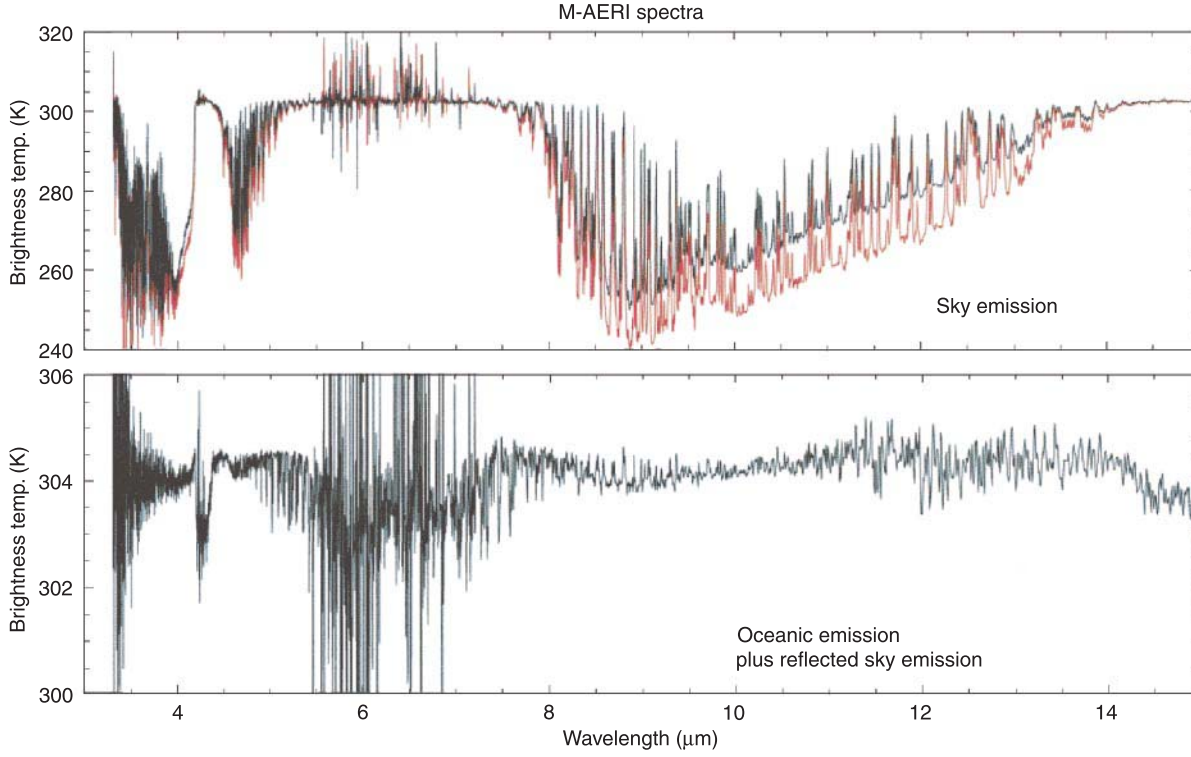

Figure 14 Spectra of emitted sky and sea view radiation measured by the M-AERI FTIR in the tropical Western Pacific Ocean on March 24, 1996. (A) Spectrum of sky radiance and (B) spectrum of corresponding sea radiance. Sky measurements were made at 45° and zenith (red) above the horizon and ocean measurements were made at 45° below the horizon. The cold temperatures in the sky spectra show where the atmosphere is relatively transparent. The 'noise' in the 5.5–7 μm range is caused by the atmosphere being so opaque that the radiometer does not 'see' clearly the instrument internal black-body targets and calibration is void. The spectrum of upwelling radiation (B) consists of emission from the sea surface, reflected sky emission and emission from the atmospheric pathlength between the sea surface and the radiometer.

(a spectral region opaque due to CO_2 emission) that are accurate to < 0.1 K.

Of considerable interest is the ability of an FTIR provide an indirect estimate of $\rho_{(\lambda,\theta)}$ so that by using eqn [5], $\varepsilon_{(\lambda,\theta)}$ can be computed. The sky radiance spectrum has particular structures associated with atmospheric emission–absorbance lines (**Figure 14A**) that are physically uncorrelated with the smooth spectrum of $\rho_{(\lambda,\theta)}$ (**Figure 4**). The spectrum of $\rho_{(\lambda,\theta)}$ can be derived by subtracting a scaled $B(T_{arm},\lambda)$ spectrum to minimize the band-limited variance of the $B(T_{sea},\lambda)$ spectrum (**Figure 14B**).

Finally, direct measurement of the thermal gradient at the air–sea interface to obtain the net heat flux has been demonstrated using an FTIR in the laboratory. The FTIR uses the 3.3–4.1 μm spectral interval that has an effective optical depth (EOD) depending on the wavelength (EOD = 0 μm at 3.3 μm whereas at 3.8 μm EOD = 65 μm) demonstrating the versatility of the FTIR. However, measurement integration times are long and further progress is required before this technique is applicable for normal field operations.

Thermal Imagers

Another recent development is the application of IR imagers and thermal cameras for high-resolution process studies such as fine-scale variability of SSST, wave breaking (**Figure 15**), and understanding air–sea gas and heat transfer. They are also used during air–sea rescue operations providing a nighttime capability for detecting warm objects such as a life raft or survivors.

These instruments use a focal plane array (FPA) detector (a matrix of individual detectors, e.g., 256×256) located at the focal point of incoming radiance together with a charge couple device that is used to 'read' the FPA. This type of 'staring array' system generates a two-dimensional image either by using a mechanical scanning system (in the case of a small FPA array) or as an instantaneous image. Larger FPA arrays are much more power efficient, lighter and smaller than more elaborate mechanical scanning systems. Rapid image acquisition (> 15 frames s^{-1}) is typical of these instruments that are available in a wide variety of spectral configurations and a typical accuracy of $\sim \pm 0.1$ K. However, considerable problems are encountered when obtaining sky radiance data due to the difficulty of geometrically matching sea and sky radiance data.

The major problem with FPA detector technology is nonuniformity between FPA detector elements and drifts in detector gain and bias. Many innovative self-calibration methods which range in quality are used to correct for these problems. For example, a small heated calibration plate assumed to be at an isothermal temperature is periodically viewed by the

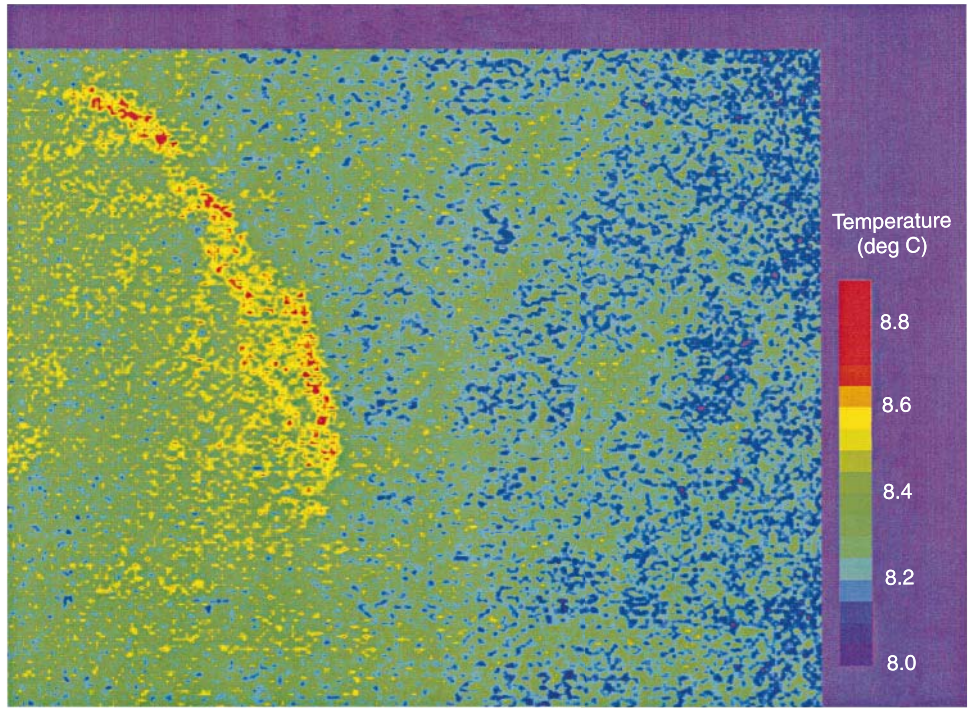

Figure 15 A thermal image of a breaking wave. Each pixel is $\sim 25 \times 25$ cm and the wavelength of the camera is 8–12 μm. (Courtesy of D. Woolf.)

detector to provide an absolute calibration. However, further development of this technology will eventually provide extremely versatile instrumentation for the investigation of fine-scale sea surface emission.

Future Direction and Conclusions

In the last 10 years, considerable progress has been made in the development and application of IR sensors to study the air–sea interface. The continued development and use of FTIR sensors will provide the capability to accurately investigate the spectral characteristics of the sea surface in order to optimize the spectral intervals used by space sensors to determine SSST. It can be expected that in the near future, new algorithms will emerge for the direct measurement of the air–sea heat flux using multispectral sounding techniques and the accurate *in situ* determination of sea surface emissivity. Although still in their infancy, the development and use of thermal cameras will provide valuable insight into the fine-resolution two-dimensional spatial and temporal variability of the ocean surface. These data will be useful in developing and understanding the sampling limitations of large footprint satellite sensors and in the refinement of validation protocols. Finally, as satellite radiometers are now providing consistent and accurate observations of the SSST (e.g., ATSR), there is a need for autonomous operational *in situ* radiometer systems for ongoing validation of their data. Such intelligent systems that are extremely robust against the harsh realities of the marine environment are currently being developed.

See also

Air–Sea Gas Exchange. Heat and Momentum Fluxes at the Sea Surface. Radiative Transfer in the Ocean. Satellite Remote Sensing of Sea Surface Temperatures. Thermohaline Circulation.

Further Reading

Bertie JE and Lan ZD (1996) Infrared intensities of liquids: the intensity of the OH stretching band revisited, and the best current values of the optical constants H_2O (1) at 25°C between 15,000 and 1 cm^{-1}. *Applied Spectroscopy* 50: 1047–1057.

Donlon CJ, Keogh SJ, Baldwin DJ *et al.* (1998) Solid state measurements of sea surface skin temperature. *Journal of Atmospheric and Oceanic Technology* 15: 775–787.

Donlon CJ and Nightingale TJ (2000) The effect of atmospheric radiance errors in radiometric sea surface skin temperature measurements. *Applied Optics* 39: 2392–2397.

Jessup AT, Zappa CJ and Yeh H (1997) Defining and quantifying micro-scale wave breaking with infrared imagery. *Journal of Geophysical Research* 102: 23 145–23 153.

McKeown W and Asher W (1997) A radiometric method to measure the concentration boundary layer thickness at an air–water interface. *Journal of Atmospheric and Oceanic Technology* 14: 1494–1501.

Shaw JA (1999) Degree of polarisation in spectral radiances from water viewing infrared radiometers. *Applied Optics* 15: 3157–3165.

Smith WL Knuteson RO, Rivercombe HH *et al.* (1996) Observations of the infrared radiative properties of the ocean – implications for the measurement of sea surface temperature via satellite remote sensing. *Bulletin of the American Meteorological Society* 77: 41–51.

Suarez MJ, Emery WJ and Wick GA (1997) The multichannel infrared sea truth radiometric calibrator (MISTRC). *Journal of Atmospheric and Oceanic Technology* 14: 243–253.

Thomas JP, Knight RJ, Roscoe HK, Turner J and Symon C (1995) An evaluation of a self-calibrating infrared radiometer for measuring sea surface temperature. *Journal of Atmospheric and Oceanic Technology* 12: 301–316.

IRON FERTILIZATION

K. H. Coale, Moss Landing Marine Laboratories, California, USA

doi:10.1006/rwos.2001.0274

Introduction

The trace element iron has been shown to play a critical role in nutrient utilization and phytoplankton growth and therefore in the uptake of carbon dioxide from the surface waters of the global ocean. Carbon fixation in the surface waters, via phytoplankton growth, shifts the ocean–atmosphere exchange equilibrium for carbon dioxide. As a result, levels of atmospheric carbon dioxide (a greenhouse gas) and iron flux to the oceans have been linked to climate change (glacial to interglacial transitions). These recent findings have led some to suggest that large-scale iron fertilization of the world's oceans